The Effect of the Anode Loading and Method of MEA Fabrication on DMFC Performance

T. V. Reshetenko[1], H.-T. Kim[1]*, U. Krewer[1], and H.-J. Kweon[1]

[1] Samsung SDI Co., LTD, 575 Shin-dong, Yeongtong-gu, Suwon-si, Gyeonggi-do, 443-391, Korea

Abstract

The influence of the Pt-Ru anode loading and MEA preparation techniques on direct methanol fuel cell (DMFC) performance is studied. Two different anode catalyst layer preparation techniques are employed. One is the direct coating of anode catalyst ink on a membrane to form a catalyst coated membrane, CCM_{anode}, and the other is the coating of the ink on the diffusion layers, which generates a catalyst coated substrate, CCS_{anode}. The power density of a combined $CCM_{anode}/CCS_{cathode}$ MEA is higher than for a $CCS_{anode}/CCS_{cathode}$ MEA. The main difference in the performance is observed in the high current density region, where two-phase flow is present and mass transfer processes govern the performance. The CCM_{anode} and CCS_{anode} have different macroscopic structures, while showing the same microscopic morphology. Based on their morphological differences, it is expected that the combination of the CCM_{anode} and carbon paper provides the more homogeneous removal of CO_2 at high currents. The authors suggest that the application of the CCM_{anode} with an optimal anode loading improves anode mass transfer, reduces methanol crossover, and enhances the electrochemical reactions.

Keywords: Direct Methanol Fuel Cell, EIS, MEA Preparation, Pt-Ru Loading

1 Introduction

The direct methanol fuel cell (DMFC) is a promising electrochemical energy source because of its low operating temperature (50–70 °C), use of liquid fuel – methanol, existing supply infrastructure, and since it has fewer safety concerns compared with the PEMFC [1–5]. Owing to these advantages, the DMFC is an appropriate power source for portable electronic devices [3, 5–7]. However, there are still a number of challenging problems to the development of such systems, which are: (i) the high electrocatalytic activity of the anode and cathode catalysts; (ii) the proton conductive membrane with high ionic conductivity and low methanol crossover, and (iii) proper water management on the cathode side [1, 2, 8–10]. Much effort has been made to find new membranes or modify the currently employed Nafion® to inhibit or reduce methanol crossover [11–13]. On the other hand, significant effort is also being devoted to electrocatalyst development [2, 8–10, 14–16]. Despite these attempts, the most prevalent DMFC electrocatalysts are still Pt-Ru black for the anode and Pt black for the cathode.

Consequently, DMFC performance can be enhanced by the optimization of the electrode structure, especially the membrane-electrode assembly (MEA) fabrication [16–19]. Commonly different coating processes are used. The first method starts with the preparation of diffusion layers (DL) with a suitable polytetrafluoroethylene (PTFE) content. Then, the catalytic material is applied to the DLs by a spraying or screen-printing technique. The MEAs are formed by hot-pressing the anode and cathode coated DL onto the proton conductive membrane. This type of MEA is denoted as the Catalyst Coated Substrate (CCS) [20, 21]. Gottesfeld [22] suggested the fabrication of MEAs by a decal method, where catalytic ink is applied to PTFE blank and subsequently transferred to the membrane. An alternative fabrication technique is the direct coating of both sides of the membrane with the catalytic materials to form Catalyst Coated Membrane (CCM) and the combination of this structure with two diffusion backings [20]. Due to the separate manufacture of the diffu-

[*] *Corresponding author, hee-tak.kim@samsung.com*

sion layers and the Catalyst coated membrane, an improved contact between the membrane, ionomer, and catalyst may be expected after hot-pressing the coated membrane. Thus, a higher efficiency is presumed for the use of the catalytic material and ionomer. The morphology of the catalyst layer is expected to vary with the MEA preparation method, even when the catalyst ink and coating method are the same. For the CCS, the catalyst layer would be coupled with a diffusion layer structure, however, for the CCM, the gas diffusion layer does not affect the catalyst layer morphology. Therefore, the effect of the MEA preparation method on performance may be analyzed considering the morphological characteristics of the catalyst layers.

The catalyst loading is an important design variable for the MEA. The loading of unsupported Pt-Ru catalyst in the anode has been reported [9, 23–27]. It was shown that Pt-Ru black with loadings higher than 8 mg cm^{-2} did not influence the cell performance [28]. Liu [24] pointed out that CCS MEAs, fabricated with unsupported Pt-Ru black, showed maximum power densities at 6 mg cm^{-2}. Considering the above-mentioned issues in catalyst layer design, our group has optimized an anode structure with a varying Pt-Ru loading and preparation method. In this paper, how these design parameters for the anode catalyst layer affect MEA performance are reported and the relationship between the anode structure and MEA performance is discussed.

2 Experimental

2.1 MEA Preparation

All the investigated MEAs were prepared with Nafion® 115 (DuPont™). The catalysts used in this work were Pt-Ru (1:1) black (HiSpec 6000, Johnson Matthey) and Pt black (HiSpec 1000, Johnson Matthey), for the anode and cathode, respectively. 10 DA (SGL, Germany), which contains 20 wt.-% PTFE, was used for the cathode diffusion layer and 10 AA (SGL, Germany), which does not contain any PTFE, was employed for the anode diffusion layer. A 1:1 (wt/wt) mixture of carbon (Vulcan XC-72, Cabot) and PTFE (Dupont™), dispersed in isopropyl alcohol, was placed on the surface of the diffusion layer (DL) to form a microporous carbon layer (MPL). The carbon loading level was controlled at 0.26 mg cm^{-2} for the anode diffusion layer and 1.3 mg cm^{-2} for the cathode diffusion layer.

Table. 1 Main characteristics of the MEA samples.

Sample	Anode				Cathode			
	Pt-Ru / mg cm^{-2}	MPL / mg cm^{-2}	Nafion® ratio	Carbon paper	Pt / mg cm^{-2}	MPL / mg cm^{-2}	Nafion® ratio	Carbon paper
CCM1a	0.67	–	0.12	SGL10AA	5.6	1.3	0.26	SGL10DA
CCM2a	1.74	–	0.12	SGL10AA	5.6	1.3	0.26	SGL10DA
CCM3a	2.03	–	0.12	SGL10AA	5.6	1.3	0.26	SGL10DA
CCM4a	3.06	–	0.12	SGL10AA	5.6	1.3	0.26	SGL10DA
CCM5a	4.52	–	0.12	SGL10AA	5.6	1.3	0.26	SGL10DA
CCM6a	6.2	–	0.12	SGL10AA	5.6	1.3	0.26	SGL10DA
CCS-ref	6.28	0.26	0.12	SGL10AA	5.6	1.3	0.26	SGL10DA

Catalyst inks, consisting of the appropriate amounts of unsupported catalyst, Nafion® solution, and isopropyl alcohol were homogenized to disperse the catalyst. For electrode preparation ($CCS_{cathode}$), the cathode catalyst ink was sprayed onto the MPL coated 10 DA. The Pt loading was 5.6 mg cm^{-2} and the Nafion® ratio was 0.26.

In this paper, the ionomer ratio in the electrode was defined as follows:

$$Nafion^{®}\ ratio = M_{Nafion®}/M_{catalyst},$$

where $M_{Nafion®}$ is the weight of dry ionomer and $M_{catalyst}$ is the weight of bulk catalyst.

The anode electrodes (CCM_{anode}) were produced by spraying the Pt-Ru catalyst ink on one side of the Nafion® 115. The Pt-Ru loading was varied from 0.67 to 6.2 mg cm^{-2} and the Nafion® ratio was 0.12. Also, a CCS_{anode} electrode was made, which was used as a reference by applying catalyst ink onto the MPL coated 10AA. The Pt-Ru loading for CCS_{anode} was 6.28 mg cm^{-2}. The catalyst and Nafion® loadings of the electrodes studied in this work are listed in Table 1.

The morphological characteristics of the catalyst layer were investigated by Scanning Electron Microscopy (JEOL JSM-6700F microscope).

The $CCS_{cathode}/CCM_{anode}$ MEAs were obtained by pressing a stack of 10DA, $CCS_{cathode}$, and CCM_{anode} at 125 °C and at 51 MPa. The $CCS_{cathode}/CCS_{anode}$ was prepared by pressing the $CCS_{cathode}$, Nafion® 115, and CCS_{anode} under the same conditions. The active cell area was 10 cm^2.

2.2 Electrochemical Characterization

Polarization curves were recorded using Wonatech Fuel Cell Test Stations. The MEAs were sandwiched between two plates with serpentine flow channels. Electrical heaters and a thermocouple were embedded in the plates for controlling the desired operating temperature. A pump was employed to supply the anode with 1 M aqueous methanol solution (*anode stoichiometry* = 3). In fuel cell mode, the cathode was fed with air at atmospheric pressure (*cathode stoichiometry* = 3). It should be noted that at current densities below 100 mA cm^{-2} the methanol flow rate was set constant (0.311 ml min^{-1}). The cell temperature was varied in the range from 50–70 °C. As a preconditioning step, the cell was operated at 0.4 V and 50 °C for 2 hrs, after which a polarization curve was recorded. This was repeated for several days. It was found that the cell performance stabilized within three days. The *I-U* curves presented here were measured after 3 days of preconditioning.

EIS (electrochemical impedance spectra) were recorded using an IM-6 (Zahner) at 50 °C in the frequency range from 100 kHz to 100 mHz. The impedance was measured with the cell under either galvanostatic or potentiostatic control.

The amplitude of the sinusoidal voltage signal did not exceed 5 mV. In order to separate the anode and cathode impedances, the anode spectrum, when the cathode was supplied with hydrogen, was recorded [29, 30]. In this way, it is possible to eliminate cathode contributions in the DMFC, since proton reduction at the cathode is much faster than methanol oxidation at the anode, therefore, the impedance contribution from the cathode can be neglected. In this configuration, the cathode acts as a reversible hydrogen electrode. The anode spectra were measured using a 2-electrode setup, using the anode and the reversible hydrogen electrode of the complete fuel cell. DMFC cathode impedance spectra were obtained as follows: the impedance spectrum of a complete DMFC, the cathode operating on air, was recorded, and then the anode spectrum was recorded as described above. The anode impedance was subsequently subtracted from the total cell impedance, resulting in a cathode impedance spectrum.

3 Results and Discussion

3.1 Effect of Pt-Ru Loading

The current-voltage curves of the MEAs with various Pt-Ru loadings are presented in Figure 1. The dependence of cell performance on Pt-Ru loading seems to vary with current density. In the low current density regime (typically ~ 90 mA cm^{-2}), the voltage at a fixed current density increased with Pt-Ru loading, but above a certain Pt-Ru loading, the performance did not increase further. At relatively high current densities (typically ~ 300 mA cm^{-2}), a different behavior was found (Table 2). The power density increased with the Pt-Ru loading up to 4.52 mg cm^{-2} and then it slightly decreased at higher Pt-Ru loadings.

To take an in-depth look into how much the electrochemical properties change with loading, EIS recorded in the low current region, where transport effects are negligible, were analyzed. Figure 2a-c shows the total, anode, and cathode impedance Nyquist plots with different Pt-Ru loadings measured at 90 mA cm^{-2}. The total impedance curves (Figure 2a) of all the studied samples were found to be made up of approximately 2 depressed semicircles, plus a pseudo-inductive loop in the low frequency region. At medium frequencies, i.e., in the range between 0.04 and 0.12 Ω (Re(Z)), the impedance decreases with increased anode catalyst loading, from 1.74 to 6.2 mg cm^{-2}, while at low frequencies the opposite tendency is observed. The same trend can also be found in the anode spectra (Figure 2b). While the low frequency region is attributed to slow methanol oxidation [31], processes like proton transport, water chemisorption, and charge/discharge processes are faster and, therefore, occur at higher frequencies. The cause of this seemingly complex loading influence, observed in the Nyquist plot, can be identified by analyzing the Bode-plot of the anode spectra (Figure 3). The angle and the absolute impedance graphs have a similar shape and size, but they are shifted to lower frequencies with increasing loading. As a result of the intersection of the shifted curves, higher loadings show lower impedances at medium frequencies but higher impedances at low frequencies. The loading only affects the frequency dependence of an EIS, not its general features. The underlying reason for the frequency shift is attributed to an increase in the active area with increasing loading. At the same current density, i.e., methanol oxidation rate, the oxidation rate per real active area decreases for higher loadings. As a result, the electrochemical processes become slower and, hence, occur at lower frequencies with increased loading. Therefore, the Bode plot may be indicative of the active surface area.

Finally, Nyquist plots for the cathode do not show a clear trend but are very close in the high and medium frequency

Table 2 Power density of the investigated MEA samples.

Sample	Pt-Ru / mg cm^{-2}	Pt / mg cm^{-2}	Power density @ 0.4 V / mW cm^{-2}		
			50 °C	60 °C	70 °C
CCM1a	0.67	5.6	36	53	73
CCM2a	1.74	5.6	56	77	96
CCM3a	2.03	5.6	56	80	96
CCM4a	3.06	5.6	56	78	99
CCM5a	4.52	5.6	76	97	116
CCM6a	6.2	5.6	69	92	116
CCS-ref	6.28	5.6	68	88	104

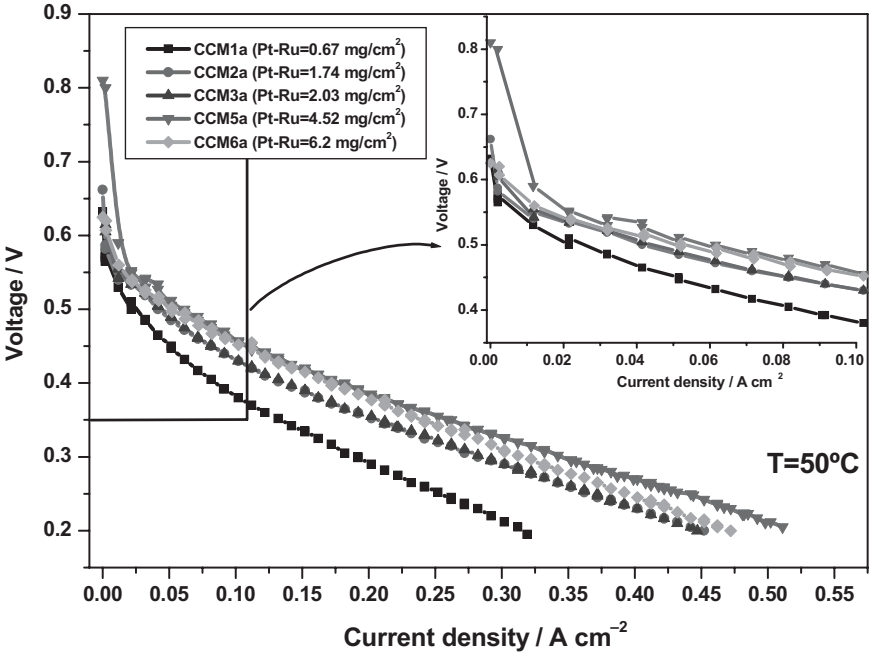

Fig. 1 Effect of Pt-Ru loading on the performance of a DMFC tested with 1 M MeOH.

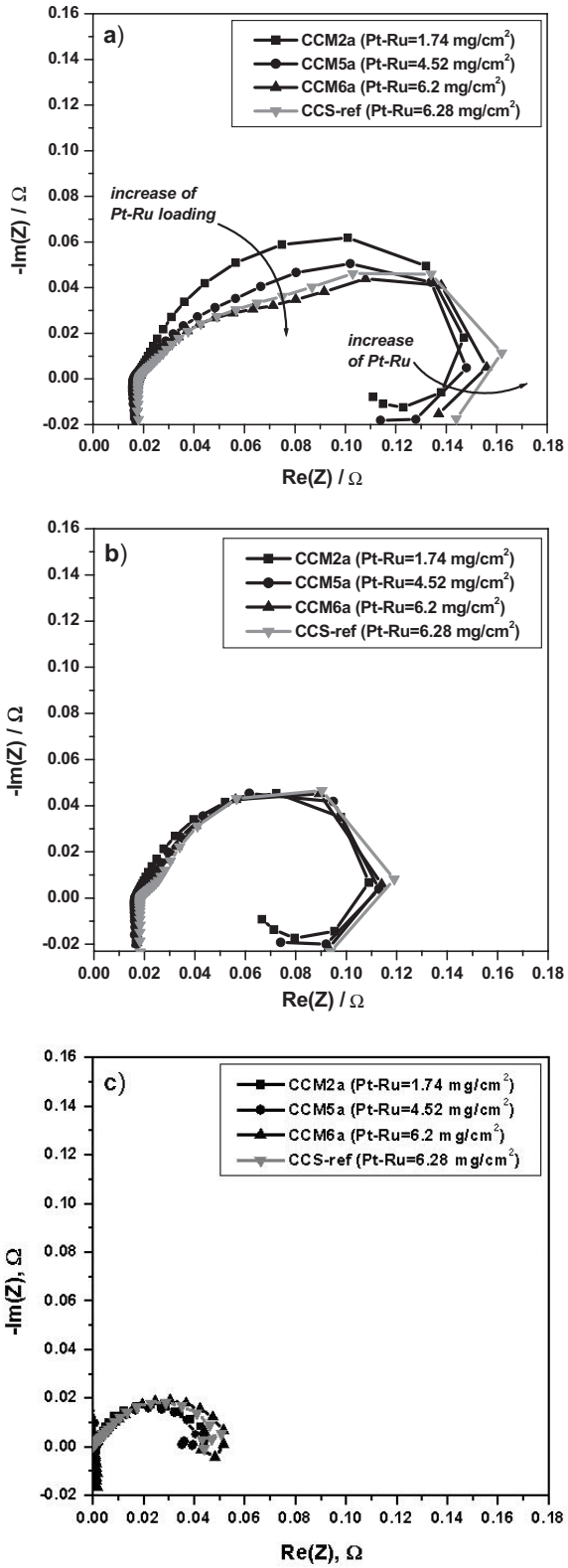

Fig. 2 Nyquist plots for the MEAs under investigation (T = 50 °C, i = 90 mA cm^{-2}): (a) total, (b) anode, (c) cathode impedance.

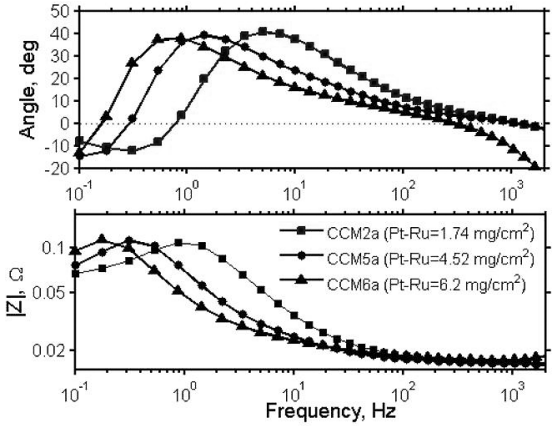

Fig. 3 Bode plots for the MEAs under investigation (T = 50 °C, i = 90 mA cm^{-2}): effect of anode loading on anode EIS.

regime. The interpretation of the low frequency region may be error-prone, since the anode EIS should also contain an impedance effect of cathodic H_2 that may distort the cathode EIS, which is calculated by subtracting the anode from the total EIS.

Although the steady state anode and total performance (Table 3) of the low loading MEA (CCM2a) is inferior compared to the higher loadings, indicators for this behaviour could not be found in any impedance spectrum. Since impedance spectroscopy is a dynamic investigation method, steady state behaviour cannot be determined; this measurement would take infinitely long.

Comparing the power densities at relatively high current density (300 mA cm^{-2}), the highest performance was observed for the CCM5a sample (Pt-Ru = 4.52 mg cm^{-2}). The CCM6a sample, with a Pt-Ru loading of 6.2 mg cm^{-2}, revealed a lower power density than CCM5a, in spite of the higher catalyst loading (Figure 1). Table 4 shows that many studies have been reported on the effect of the Pt-Ru content, but the best results were observed at different loadings and operating conditions. Consequently, it is difficult to compare the current results with published data [19, 23–27]. Nevertheless, in the study presented here, the CCM5a (Pt-Ru = 4.52 mg cm^{-2}) has a significantly better performance at low temperatures, compared with the reported data.

The catalysts active sites and the active surface area of the electrode are assumed to increase with catalyst loading, which could reduce the activation overpotential at the anode. On the other hand, the thickness of the catalyst layer increases with catalyst content, and the concentration overpo-

Table 3. EIS characterization of the MEAs.

Parameter	CCM2a	CCM5a	CCM6a	CCS-ref
R_{el} / Ω·cm^2	0.168	0.164	0.177	0.184
OCV / V	0.662	0.652	0.670	0.655
Total / V (i = 90 mA cm^{-2})	0.431	0.461	0.459	0.472
Anode / V (i = 90 mA cm^{-2})	0.409	0.378	0.380	0.361
Cathode / V (i = 90 mA cm^{-2})	0.840	0.839	0.839	0.833

Table 4. Comparison of the data obtained with published results.

Sample	MEA type	Pt-Ru / mg cm^{-2}	Pt / mg cm^{-2}	Membrane	C_{CH3OH} / M	Oxidizing agent	T / °C	Power density @ 0.4 V / mW cm^{-2}
CCM5a	CCM	4.52	5.6	Nafion® 115	1	air	70	116
MEA [19]	CCS	3.0	3.0	Nafion® 115	1	air	90	40
	CCM	3.0	3.0	Nafion® 115	1	air	90	126
MEA [23]	CCS	5.0[1]	3.0	Nafion® 115	2	air	80	44
MEA [24]	CCM	6.0	6.0	Nafion® 117	0.5	O_2	90	160
MEA [25]	CCM	7.8	7	Nafion® 117	1	air-breathing	22	12
MEA [26]	CCS	3.75[2]	1.0	Nafion® 117	2	O_2	80	64
MEA [27]	CCM	1.5-3.0	2.46	Nafion® 117	1	O_2	75	100

[1] 80% (Pt-Ru)/C
[2] Pt(54%)-Ru/C supported catalyst, Pt/Ru=1.5 (TEC61E54, Tanaka)

tential increases due to the mass-transfer limitations of Methanol/CO_2 through the thicker catalyst layer at the anode at high current density. The limited "penetration depth" of the electric field is considered [32]. If the thickness of the catalyst layer exceeds the penetration depth, the electrochemical reaction predominantly takes place in the inner part of the catalyst layer, whereas, the outer part is less active and a further increase of the loading and layer thickness can lead to MeOH/CO_2 transfer limitations.

This means that mass transfer limitations would dominate at a high anode loading level, but at a low catalyst content sluggish methanol oxidation could be observed. Therefore, it was found that an anode loading of 4.52 mg cm^{-2} is likely to be a reasonable compromise between these two significant difficulties encountered during DMFC operation.

3.2 Effect of Anode Structure

According to the SEM images of the CCM_{anode} and CCS_{anode} (Figure 4), it is possible to distinguish 2 levels of electrode structure:

(i) Microscopic, which is determined by the catalyst ink properties (e.g., size of catalyst agglomerates) and the coating technique;
(ii) Macroscopic, which is controlled by structural and textural properties of the substrate (membrane or carbon paper).

A comparison of the CCM_{anode} and CCS_{anode} shows that the microscopic structures of these electrodes are the same but significant differences are observed on the macroscopic level. As can be seen from Figure 4, the CCM_{anode} (Figure 4a-c) is characterized by a very dense catalyst layer on the membrane surface, whereas the CCS_{anode} (Figure 4d,e) has a structure which is strongly affected by the carbon paper. Thus, the CCS_{anode} is a very porous electrode, with a pore size of 10–100 μm; these pores can extend through the whole depth of the electrode.

In order to elucidate the effect of the preparation technique, the performance of the CCM6a and CCS-ref samples, which feature the same anode and cathode loadings, has been compared. Table 2 shows that the power densities of the $CCS_{cathode}/CCM_{anode}$ MEA, containing 4.52 mg cm^{-2} of Pt-Ru, are higher than observed for the CCS-ref MEA with an anode loading of 6.28 mg cm^{-2}. The power density of the CCM6a only exceeds the CCS-ref performance at high operating temperatures. Figure 5 presents the *I-U* curves for the MEAs at 50 and 70 °C. At low current densities the performances of the samples are almost the same, which is also confirmed by EIS data, as shown in the following.

Due to the similar loading of the CCS-ref and CCM6a sample, a comparison between the impedance spectra recorded at low current densities should clarify the electrochemical effect of the MEA fabrication method. As discussed previously, the CCS and CCM have completely different macroscopic structures, while showing the same microscopic morphology. In the total EIS and the anode EIS (Figure2a,b), just a slightly lower resistance for the CCS-ref is observed, while the cathode EIS (Figure 2c) seem to be identical (low frequency

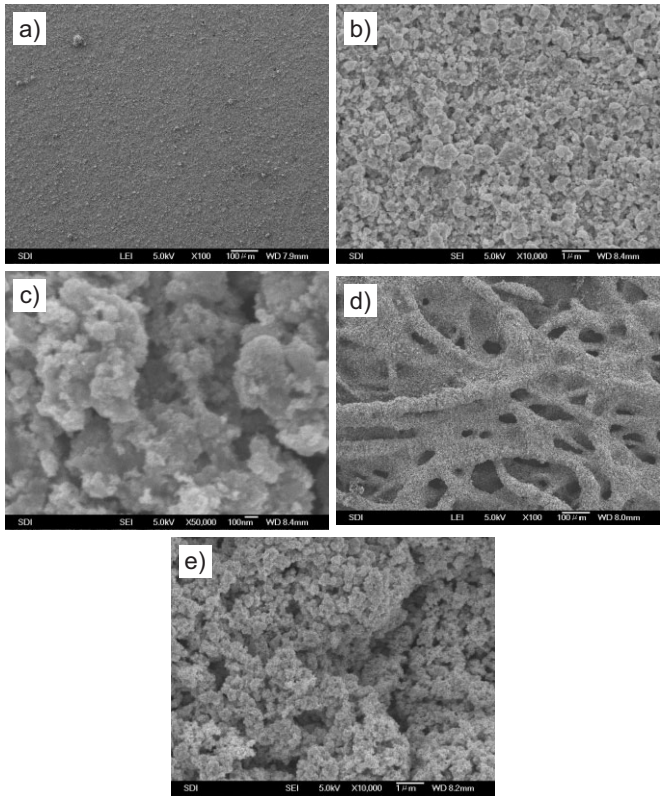

Fig. 4 SEM images: (a), (b), (c) CCM_{anode}; (d), (e) CCS_{anode} (Pt-Ru black catalyst).

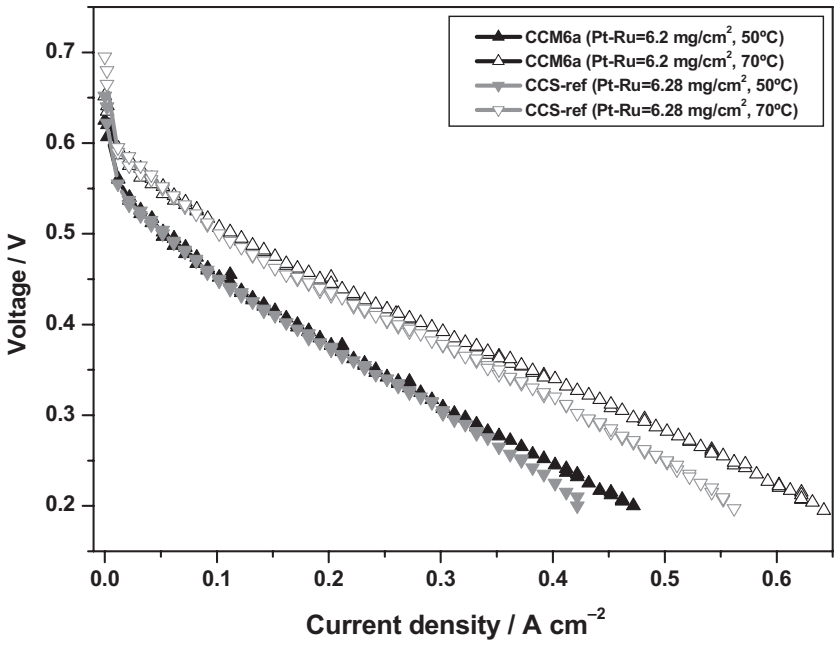

Fig. 5 Polarization curves of the CCM6a and CCS-ref samples (1 M MeOH, T = 50 °C, 70 °C).

region not considered as discussed above). In the case where the MEA fabrication method, and hence the macroscopic morphology, has little effect on the anode catalyst layer performance at the given current density, similar Bode plots should be obtained. This is the case, as shown in Figure 6. The angle and absolute impedance graphs of both MEAs are overlapping except at high frequencies. There, the CCS-ref sample shows a higher absolute resistance, indicating a poorer contact between the catalyst layer and membrane (additional artifact at angle < 0: cable inductance). Therefore, analysis suggests that the EIS and electrochemical performance at low current densities are dominated by the microscopic structure, which seems to be identical for both MEA fabrication methods. This explains the previously discussed similar steady state *I-U* performances for the CCM and CCS at low current densities (Figure 5, Table 2).

Table 3 shows the values of the anode and cathode potentials during the measurements. The CCM_{anode} samples demonstrate slightly higher cathode potentials, when compared with the CCS-ref, which may serve as evidence of decreasing methanol crossover. It seems reasonable to suggest that the CCM designed anode is preferable for DMFC applications, since this structure should reduce methanol penetration from the anode to the cathode side. In addition, some methanol is consumed in the outer part of the anode layer, and as a consequence, the cathode reaction is likely to be improved [27, 33].

Here, the *I-U* curves (Figure 5) show a stronger deviation, which may be attributed to different mass-transfer characteristics for the fabricated MEAs. As observed in Figure 4, the macroscopic structure of the CCM_{anode} and CCS_{anode} are completely different. The CCM_{anode} shows a dense structure with pore sizes below 1 μm (Figure 4a), while the supporting carbon paper has pore sizes in the range from 10–100 μm [34]. On the other hand, the macroscopic structure of the CCS_{anode} seems to be a continuation of the carbon paper structure on which it was sprayed. Its pore size, as well as its structure, strongly resembles that of the carbon paper. This difference in structure should have an effect on the mass transfer characteristics, especially if two-phase flow is present. As observed by Scott et al. [35] and Lu et al. [34], the CO_2 gas evolution pattern at the surface of a DMFC anode DL strongly depends on the structure and morphology of the applied carbon paper. Cells using carbon paper generated large CO_2 bubbles, which formed large and discrete gas slugs in the channel, and the more homogeneously structured carbon cloth produced relatively small gas bubbles, which detached more easily. An analogy can be drawn to this for the influence of the macroscopic morphology of a catalyst layer. In principle, three different kinds of anode structures exist, as illustrated in Figure 7. First, a dense anode with pores much smaller than in the DL (left), which was found for the CCM anodes presented here. Secondly, a porous anode, which has a structure that differs from that of the carbon paper (middle). Finally, a porous anode, where the DL structure continues (right). The latter is observed for the CCS_{anode}. At low currents, only a small amount of CO_2 is generated and the gas accumulates in the outer part of the DL, where the bubbles grow and finally detach into the channel. The influence of CO_2 bubbles aggregating in the DL on the catalyst layer performance may be assumed to be negligible, since CO_2 removal is sufficiently fast (Figure 7a). In contrast,

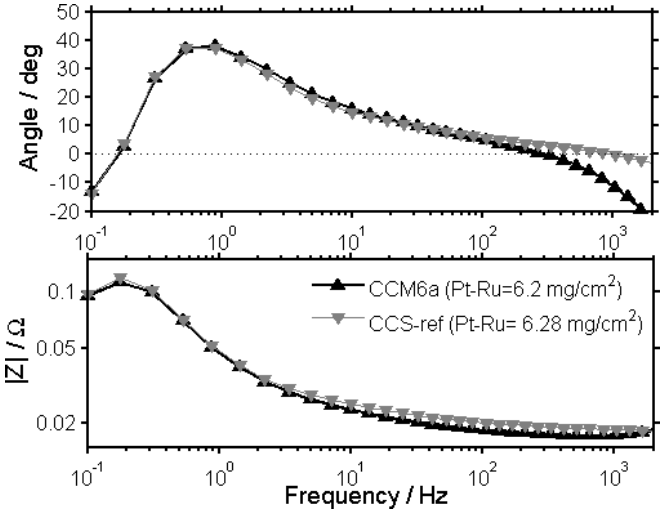

Fig. 6 Bode plots for the MEAs under investigation (T = 50 °C, i = 90 mA cm^{-2}): effect of anode preparation method on anode EIS.

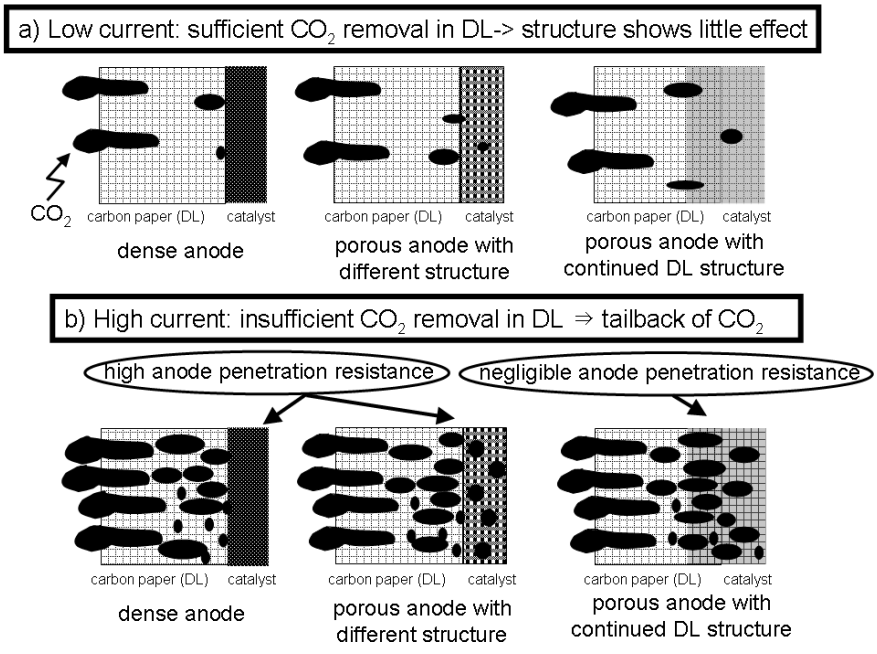

Fig. 7 Interaction between anode structure and carbon paper DL: effect on CO_2 removal.

at high currents, where vast amounts of CO_2 are generated, the periodic removal of CO_2 from the DL should lead to an increased accumulation of gas in the DL, leading to a CO_2 holdup. Here, a dense anode catalyst layer poses a strong resistance to the penetration of large CO_2 bubbles (Figure 7b, left). A similar behaviour might be expected for the porous anode catalyst layer with a macroscopic structure differing from the DL. The location and shape of the pores do not continue at the interface (Figurte 7b, middle). In contrast to this, since the pore shape, as well as the pore location, is continuous from the DL to the catalyst layer for the CCS type MEAs, the anode catalyst layer should exhibit only a small CO_2 penetration resistance. As a result, the CO_2 holdup at high currents may lead to decreasing mass transfer in the CCS design and, hence, to the observed lower IV performance at higher currents. More drastically this phenomenon is pronounced at the highest operating temperature, 70 °C (Figure 5). Here, more gaseous CO_2 is present due to the lower solubility of CO_2 in water.

4 Conclusions

In this paper, the effects of the anode loading and anode fabrication technique (CCM or CCS) on DMFC performance were investigated. It was shown that the application of a CCM method for anode manufacture demonstrated higher performance in comparison with the CCS method. The power density of the combined $CCM_{anode}/CCS_{cathode}$ MEA was higher than for the CCS MEA and can reach 116 mW cm^{-2} at 70 °C and a Pt-Ru loading of 4.52 mg cm^{-2}. The main difference in the performance of the $CCM_{anode}/CCS_{cathode}$ MEA and CCS MEA was observed in the high current density region, where two-phase (methanol solution/CO_2) flow was present and mass transfer processes started to become influential. According to SEM data, the CCM_{anode} and CCS_{anode} featured different macroscopic structures, while showing the same microscopic morphology. The CCS_{anode} seemed to be a continuation of the porous carbon paper structure on which it was sprayed. In contrast to this, the CCM_{anode} had a relatively dense structure. It was suggested that the combination of the CCM_{anode} and DL could provide a more homogeneous removal of CO_2 at high currents, while for the CCS_{anode} CO_2 holdup in the catalyst layer could be expected. This may result in reduced mass transfer and lower power densities. The application of the CCM_{anode} with optimal anode loading seemed to improve anode mass transfer, reduce methanol crossover, and enhance the electrochemical reactions. Therefore, the CCM design of the MEA is likely to be a promising way to enhance DMFC performance.

Acknowledgements

We are grateful to Dr. Hankyu Lee and Dr. Moonyup Jang for the production of the CCS.

References

[1] A. K. Shukla, A. S. Arico, V. Antonucci, *Renewable Sustainable Energy Rev* **2001**, *5*, 137.
[2] A. S. Arico, S. Srinivasan, V. Antonucci, *Fuel Cells* **2001**, *1*, 133.
[3] H. Dohle, H. Schmitz, T. Bewer, J. Mergel, D. Stolten, *J. Power Sources* **2002**, *106*, 313.
[4] A. Blum, T. Duvdevani, M. Philosoph, N. Rudoy, E. Peled, *J. Power Sources* **2003**, *117*, 22.
[5] C. Y. Chen, P. Yang, Y. S. Lee, U. F. Lin, *J. Power Sources* **2005**, *141*, 24.
[6] C. Xie, J. Bostaph, J. Pavio, *J. Power Sources* **2004**, *136*, 55.
[7] J. Han, E.-S. Park, *J. Power Sources* **2002**, *112*, 477.
[8] A. Hamnett, *Catalysis Today* **1997**, *38*, 445.
[9] M. P. Hogarth, T. R. Ralph, *Platinum Metals Rev.* **2002**, *46*, 146.
[10] T. Schultz, S. Zhou, K. Sundmacher, *Chem. Eng. Technol.* **2001**, *24*, 12.
[11] M. Walker, K. M. Baumgartner, M. Kaiser, J. Kerres, A. Ullrich, E. Rauchle, *J. Appl. Polymer Sci.* **1999**, *74*, 67.
[12] J. A. Kerres, *J. Membrane Sci.* **2001**, *185*, 3.

[13] V. Baglio, A. S. Arico, A. DiBlasi, V. Antonucci, P. L. Antonucci, S. Licoccia, E. Traversa, F. Serraino Fiory, *Electrochem. Acta* **2005**, *50*, 1241.
[14] V. Rao, P. A. Simonov, E. R. Savinova, G. V. Plaksin, S. V. Cherepanova, G. N. Kryukova, U. Stimming, *J. Power Sources* **2005**, *145*, 178.
[15] A. S. Arico, C. Creti, H. Kim, R. Mantegna, N. Giordano, V. Antonucci, *J. Electochem. Soc.* **1996**, *143*, 3950.
[16] *Handbook of Fuel Cells*, Vol. 4 (Eds. W. Vielstich, A. Lamm, H. A. Gasteiger), John Willey & Sons, **2002**.
[17] Z. Wei, S. Wang, B. Yi, J. Liu, L. Chen, W. Zhou, W. Li, Q. Xin, *J. Power Sources* **2002**, *106*, 364.
[18] A. Lindermeir, G. Rosenthal, U. Kunz, U. Hoffman, *J. Power Sources* **2004**, *129*, 180.
[19] S. Q. Song, Z. X. Liang, W. J. Zhou, G. Q. Sun, Q. Xin, V. Stergiopoulos, P. Tsiakaras, *J. Power Sources* **2005**, *145*, 495.
[20] *Handbook of Fuel Cells*, Vol. 3 (Eds. W. Vielstich, A. Lamm, H. A. Gasteiger), John Willey & Sons, **2002**.
[21] E. A. Ticianelli, C. D. Derouin, A. Redondo, S. Srinivasan, *J. Electrochem. Soc.* **1988**, *135*, 2209.
[22] W. S. Wilson, S. Gottesfeld, *J. Electrochem. Soc.* **1992**, *139*, L28.
[23] J. S. Lee, K. I. Han, S. O. Park, H. N. Kim, H. Kim, *Electrochem. Acta* **2004**, *50*, 807.
[24] L. Liu, C. Pu, R. Viswanathan, Q. Fan, R. Liu, E. S. Smotkin, *Electrochem. Acta* **1998**, *43*, 3657.
[25] C. Y. Chen, P. Yang, Y. S. Lee, K. F. Lin, *J. Power Sources* **2005**, *141*, 24.
[26] N. Nakagawa, Y. Xiu, *J. Power Sources* **2003**, *118*, 248.
[27] X. Zhao, X. Fan, S. Wang, S. Yang, B. Yi, Q. Xin, G. Sun, *Int. J. Hydrogen Energy* **2005**, *30*, 1003.
[28] S. Surampudi, S. R. Narayanan, E. Vamos, H. Frank, G. Halpert, A. La Conti, J. Kosek, G. K. Surya Prakash, G. A. Olah, *J. Power Sources* **1994**, *47*, 377.
[29] J. T. Mueller, P. M. Urban, *J. Power Sources* **1998**, *75*, 139.
[30] J. T. Mueller, P. M. Urban, W. F. Hoelderich, *J. Power Sources* **1999**, *84*, 364.
[31] U. Krewer, M. Christov, T. Vidakovic, K. Sundmacher, *J. Electroanal. Chem.* **2006**, *589*, 148.
[32] J. Divisek, R. Jung, I. C. Vinke, *J. Appl. Electrochem.* **1999**, *29*, 165.
[33] A. Havranek, K. Klafki, K. Wippermann, *Proceedings of the Second Advanced Batteries and Accumulators*, Brno, Czech Republic, **2001**, pp. 32.
[34] G. Q. Lu, C. Y. Wang, *J. Power Sources* **2004**, *134*, 33.
[35] K. Scott, W. M. Taama, P. Argyropoulos, *J. Power Sources* **1999**, *79*, 43.